Received: 27 August 2020 | Revised: 25 January 2021 | Accepted: 27 January 2021

DOI: 10.1002/esp.5089

RESEARCH ARTICLE

ESPL WILEY

Mapping mineralogy in evaporite basins through time using multispectral Landsat data: Examples from the Bonneville basin, Utah, USA

Mark H. Radwin[1] | Brenda B. Bowen[1,2]

[1]Department of Geology and Geophysics, University of Utah, Salt Lake City, Utah, USA

[2]Global Change and Sustainability Center, University of Utah, Salt Lake City, Utah, USA

Correspondence
Mark H. Radwin, Department of Geology and Geophysics, University of Utah, 115 South 1460 East, Frederic A. Sutton Building 205, Salt Lake City, UT 84112, USA.
Email: mark.radwin@utah.edu

Funding information
National Science Foundation

Abstract

The Bonneville basin, located in north-western Utah, is a vast evaporite basin which is home to the world-renowned Bonneville Salt Flats international speedway and is a highly valued landscape undergoing rapid change and anthropogenic influence. Air quality, snowpack, the local hydrological system, and state tourism are all impacted by the nature of the surface sediments exposed in the Bonneville basin. Mapping the Bonneville basin over time with remote sensing methods provides insight into the dynamics and impacts of the changing surface landscape. Utilizing the Landsat-5 Thematic Mapper (TM) and Landsat-8 Operational Land Imager (OLI) sensors, a set of band math indices are empirically established to map the predominant halite, gypsum, and carbonates mineralogical zones of the Bonneville basin. Spectral comparisons of representative samples from the study area and image-derived spectra indicate the halite of the Bonneville basin is wet and that gypsum deposits are slightly mixed with halite. The established indices are assessed in four ways, all of which support the ability of the indices to accentuate the associated mineralogical endmembers. Two study areas within the Bonneville basin are investigated temporally from 1986, 1995, 2005, and 2016 and show changing patterns in mineral distribution that align with surface processes active through these timescales. These indices provide a resource for mapping mineralogy though time in evaporite basins globally with diverse applications for questions about land use and environmental change.

KEYWORDS
band math operations, Bonneville basin, Bonneville Salt Flats, evaporite basins, evaporites, multispectral Landsat data, playas

1 | INTRODUCTION

The Bonneville basin, located in north-western Utah, western United States, is the largest modern evaporite basin of North America with an extent of ~9920 km^2 and is covered by Pleistocene Lake Bonneville deposits. Lake Bonneville was the largest Pleistocene lake in the Great Basin region and had a surface area of 51,300 km^2 at its maximum extent (Oviatt, 1997; Benson *et al*., 2011). Modern remnants of Lake Bonneville are observable as the Great Salt Lake, Bonneville basin, and shoreline features throughout northern Utah. The landscape of the basin includes very flat topography interrupted by juxtaposed bedrock and dune features (Eardley, 1962; Dean, 1978). Isostatic rebound from the disappearance of Lake Bonneville has resulted in a slight westward tilt (Eardley, 1962; Crittenden, 1963). The Bonneville basin, commonly referred to as the Great Salt Lake Desert, contains many separated but linked subregions (Figure 1); the Bonneville Salt Flats, the Newfoundland basin, Pilot Valley, the Dugway Proving Grounds (military testing site), and

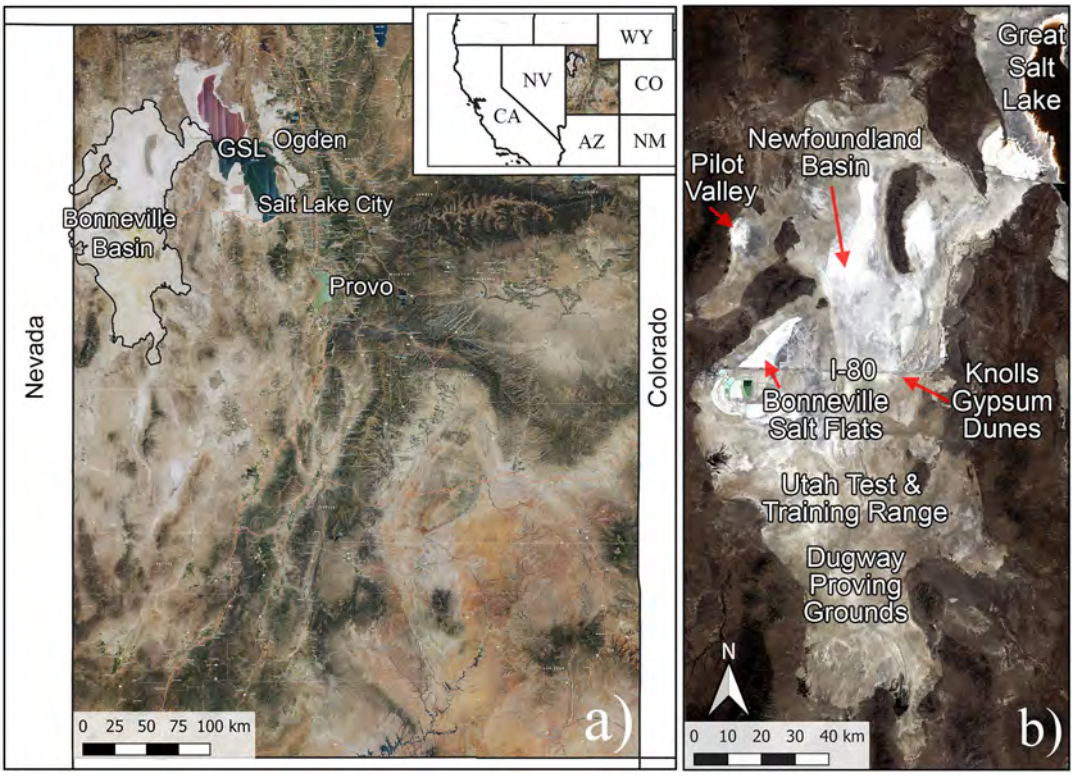

FIGURE 1 (a) Map of Utah illustrating the extent of the Bonneville basin, located in north-western Utah, with a surface area of ~9920 km^2. Basemap is from the Utah Automated Geographic Reference Center (AGRC). GSL is the Great Salt Lake. (b) 2016 Landsat-8 OLI image of the Bonneville basin, with identified sub-regions. Center of basin, along I-80, is located at 40.732°N and 113.609°W. Datum is WGS 84 EPSG:3857

the Utah Test and Training Range (military testing site). Although a suite of minerals commonly found in evaporite basins are present (Foshag, 1926; Lowenstein & Hardie, 1985) in the Bonneville basin (Figure 2), predominant evaporites present on the surface are halite and gypsum, where gypsum occurs along the margins of salt crusts as well as in extensive dune fields in the central and eastern areas of the basin. The evaporites are a superficial cap to more regionally extensive and deeper lacustrine carbonate and carbonate-clay deposits (Lines, 1979; Mason & Kipp, 1998; Kohler, 2002; Jones *et al*., 2009).

The Bonneville Salt Flats, a large perennial salt crust transected by Interstate-80 (I-80), is located in the central western side of the basin and attracts motorsport enthusiasts from around the world as it can provide a unique and accessible surface for racing during dry summers (Bowen *et al*., 2018). A shallow-brine aquifer that saturates the salt crust has been exploited for large-scale commercial extraction of halite and potash since the early 1900s Mason & Kipp, 1998; (Lines, 1979). Furthermore, the Bonneville Salt Flats are an important recreation site used for travel, art, film making, and scientists, such that it is designated on the US National Register of Historic Places. Commonly, salt crusts form in the central low-point of evaporite basins, however, fluid dissolution linked with isostatic tilting has migrated the salt crust and basin low-point westward (Eardley, 1962; Crittenden, 1963).

In 1986, in response to high Great Salt Lake water levels, the Great Salt Lake pumping project was initiated which pumped 695 million tons of brine into the Newfoundland basin, the northern central part of the Bonneville basin, and subsequently formed a 10 million ton anthropogenic salt crust northeast of the Bonneville Salt Flats (Kohler, 2002; Jones *et al*., 2009). A third salt crust intermittently exists in the northwest region of the basin in Pilot Valley, where there is a lack of human disturbance (Lynch *et al*., 2015). The southern part of the Bonneville basin is predominantly government land used for military testing, but is broken into the Dugway Proving Grounds and Utah Test and Training Range. Collectively, these two testing sites encompass the largest span of special use airspace in the United States.

Gypsum dunes are distributed along the eastern side of the basin, notably proximal to the Knolls Recreation Area, and predominantly accumulate in the areas of highest isostatic uplift (Eardley, 1962). The base elevation at Knolls is about 5 m higher in elevation than the Bonneville Salt Flats crust. Gypsum dunes are also located throughout the Newfoundland basin (Jones *et al*., 2009). It is thought the dunes originate from the ablation of surface gypsum crystals that have precipitated from sulfate rich pore-fluids which reach the surface through capillary processes or via displacive growth (Eardley, 1962; Bowen *et al*., 2018). Additionally, layers of gypsum sand interbedded within the Bonneville Salt Flats halite crust suggests there were gypsum dunes at the present location of the Bonneville Salt Flats prior to the westward mobilization of the halite crust or that local springs have focused gypsum rich brines into the subsurface (Eardley, 1962; Bowen *et al*., 2018). Construction of a draft fence by the Western Pacific Railroad Company in 1952 resulted in new dune features North of I-80, illustrating anthropogenic influence on gypsum dune distribution within the Bonneville basin (Eardley, 1962).

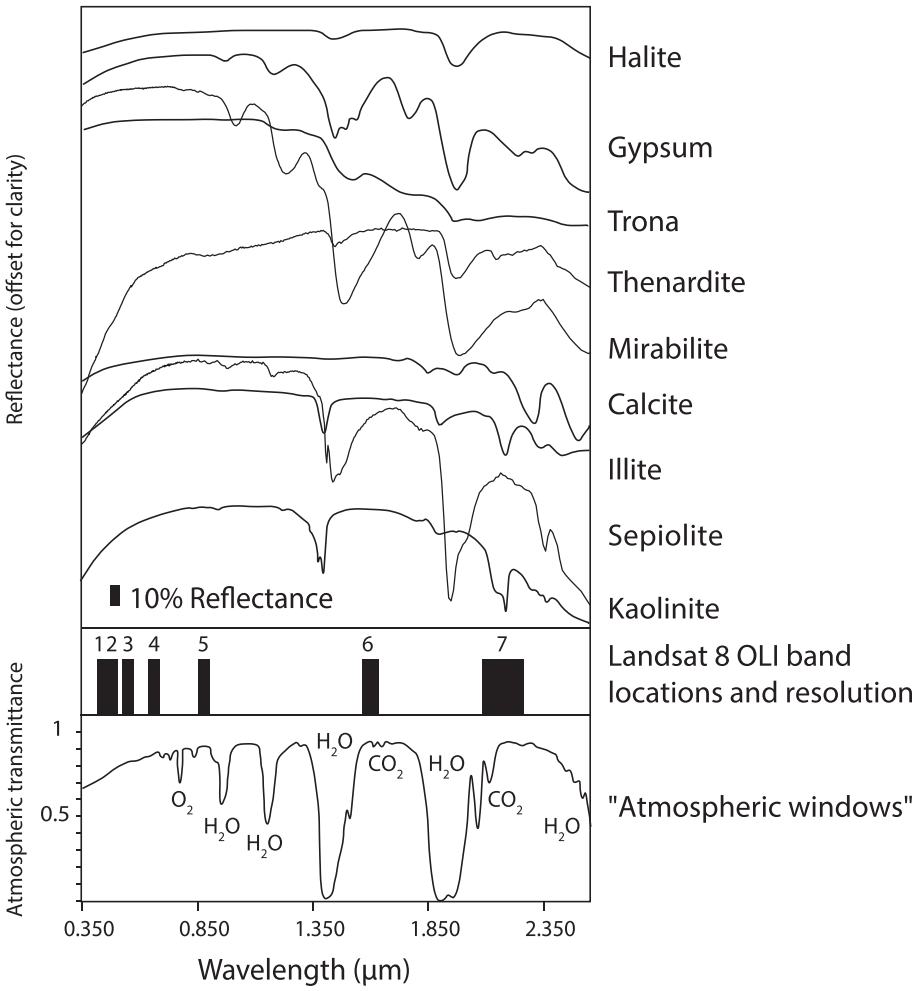

FIGURE 2 Reflectance spectra of common global evaporite basin mineralogies correlated with the spectral resolution and wavelengths of the Landsat-8 OLI sensor. An atmospheric transmittance plot at the bottom shows locations of atmospheric absorption bands. Modified from Clark *et al*. (2007)

Carbonate lacustrine sediments in the Bonneville basin are deposits from Lake Bonneville and underlie all of the evaporites (Eardley, 1962; Lines, 1979; Mason & Kipp, 1998; Gilbert, 1890; Jones *et al*., 2009). These carbonates are composed of clay-sized calcite, aragonite, dolomite, sand sized oolites, and various phyllosilicate minerals (Eardley, 1962; Lines, 1979; Jones *et al*., 2009; Bowen *et al*., 2018). Multiple types of carbonate-clay surfaces have been recognized within the basin, being initially differentiated by appearance and apparent moisture content (Lines, 1979; Jones *et al*., 2009; Lynch *et al*., 2015).

1.1 | Importance of studying the Bonneville basin

Evaporite basins such as the Bonneville basin are important to study and monitor as they have implications for land use, public health, and economic resources. However, surface processes in evaporite basins, specifically related to changes in distribution over time and in response to climate change and land-use management practices, are not well understood. Previous work in the Bonneville basin established that mineralogical distribution is the result of concentric evaporative zonation, where there is a chloride zone, gypsum zone, and carbonate zone (Lines, 1979). However, current surface sediment distribution as well as mineralogical characteristics (mixing of mineralogies) of the Bonneville basin suggest much of the surface has been greatly modified by aeolian processes, erosion, reworking, redeposition, and weathering (Bowen *et al*., 2017).

Air quality in arid regions containing evaporite basins is influenced by mineralogy and surface processes in these basins, as they are major sources of dust particles and evaporite crusts can help to prevent entrainment of aeolian particles (Gill, 1996; Pelletier & Cook, 2005; McLaurin *et al*., 2011; Quick & Chadwick, 2011). In Utah, the largest regional contributor to dust is the Bonneville basin, which can have adverse effects on air quality and also acts to compromise the snowpack in and around the Wasatch mountains by accelerating snow melt (Hahnenberger & Nicoll, 2014; Skiles *et al*., 2018; Goodman *et al*., 2019). Utah relies on its snowpack for water, and much of Utah's economy is fed by ski-resort related tourism. Dust events can compromise soils and vegetation downwind, posing a threat to the agriculture in the Salt Lake Valley. Better understanding of the surface processes driving aeolian transport and dust emission in the Bonneville basin will aid in determination of possible remediation techniques for dust prevention, such as utilizing salt crusts to prevent mobilization of fine sediments.

Anthropogenic impacts on evaporite basins have been observed; these impacts include lowering of groundwater levels, accelerating desiccation, triggering aeolian transport of fine surface sediments, affecting albedo of surface mineralogies, and reduction of vegetation cover (vegetation helps to prevent wind erosion) (Gill, 1996). It is important to quantify the influence of

anthropogenic activities in the Bonneville basin, as it is heavily disrupted by anthropogenic use and is closely coupled to regional hydrology and climate. The motorsport community has voiced concerns that the Bonneville Salt Flats salt crust has been shrinking over time and previous work has verified a shrinking extent of the salt crust (Mason & Kipp, 1998; Bowen *et al*., 2017). The specific processes leading to the decrease in salt extent are not well-documented, but it is hypothesized and generally believed that extraction of the brine associated with the salt crust is the primary cause (Lines, 1979; Mason & Kipp, 1998; Bowen *et al*., 2018). The Bureau of Land Management designated the Bonneville Salt Flats as an Area of Critical Environmental Concern in 1985, yet there is a need to better understand the surface dynamics of the Bonneville basin to make optimal management decisions. The changing conditions at the Bonneville Salt Flats continues to raise concerns with the public, motorsport community, media, government land-use management organizations, scientific community, and mine operators. Additionally, assessing the impact and evolution of introducing 695 million tons of brine to Newfoundland basin in the mid-1980s has not been studied in depth (Bureau of Land Management, 1986; Kohler, 2002; Jones *et al*., 2009). It is unknown how the 10-million-ton anthropogenic salt crust created by the introduced brine will evolve over time, given that it is a landscape that is highly modified by land management decisions in addition to geological processes.

1.2 | Mapping the Bonneville basin

Spatiotemporal evaluation of the Bonneville basin is needed to better understand the surface dynamics and changes within the basin that are related to climate change and anthropogenic use. In turn, a deeper understanding of landscape processes which impact society may be achieved. Field observations on an appropriate scale are challenging, as transportation in the basin is difficult, the study area is very large, much area is restricted to military use, and surface sediment distribution of materials can change rapidly due to events such as flooding (Craft & Horel, 2019). Thus, remote sensing techniques are ideal for consistent mapping of evaporite and carbonate surface sediment distribution through time. Time series analysis of surface sediment distribution maps provide insights into the processes and controls on their distribution, and can contribute to quantitative estimates of rates of surface change over decadal timescales. Previous works have utilized hyperspectral optical sensors for the mapping of evaporites, which provide high spectral resolution and therefore more accurate mineral identification, however, current hyperspectral sensors lack consistent and recurring temporal coverage at high spatial resolution (Moersch *et al*, 2001; Milewski *et al*., 2017). There is a lack of available hyperspectral data for the Bonneville basin, as scenes have either yet to be captured over the basin for specific sensors or are too spatially limited or cloudy to be of use for mapping (i.e., Hyperion data up to 2020). Multispectral optical sensors commonly revisit the same location within weeks and offer moderate to high spatial resolution, yet contain orders of magnitude lower spectral information. Previous studies have utilized multispectral sensors to map evaporite basins throughout the world, and have shown there is enough spectral information captured by multispectral sensors to effectively discriminate between some compositional endmembers (Mohammad *et al*., 2001; Li *et al*., 2014; Bowen *et al*., 2017; Flahaut *et al*., 2017; Soltaninejad & Ranjbar, 2018; Gürbüz, 2019; Milewski *et al*., 2020). The majority of multispectral methodologies utilized in past studies for the mapping of evaporite basins are Maximum Likelihood Classification (MLC), Sequential Maximum Angle Convex Cone (SMACC), Spectral Angle Mapper (SAM), band ratio image composites, decorrelation stretching, and principal component analysis (PCA) (Moersch *et al*., 2001; Mohammad *et al*., 2001; Li *et al*., 2014; Flahaut *et al*., 2017; Soltaninejad & Ranjbar, 2018; Gürbüz, 2019; Milewski *et al*., 2020). Of these methods, only band ratios act to target spectral features of interest by amplifying or subduing spectral contrast (difference in reflectance) between bands of interest. The present work builds on recent related research by Bowen *et al*. (2017), utilizing Landsat data to map halite extent at the Bonneville Salt Flats from 1986 to 2015 using a band math operation that was established through an iterative combination of field-based spectral and mineralogical observations, and image-derived spectral analysis. This new work introduces a band math index method for mapping halite, gypsum, and carbonates within the entire Bonneville basin utilizing Landsat data, and applies these indices over time to observe changes in surface sediment distribution over regional scales. The presented indices are limited by their multispectral nature and may be compromised by sub-pixel mixing, bedrock, vegetation, moisture variability, anthropogenic infrastructure, and the presence of minerals other than the chosen endmembers. Furthermore, the lack of usable hyperspectral data has presented a challenge to validate the indices. Thus, the presented indices, although useful for understanding the general surface sediment distribution, should be used with discretion. Band math operations provide the benefit of targeting specific spectral features of interest as well as being easily reproducible. Sample-based laboratory spectra and image-derived reflectance spectra are analyzed and compared to assess spectral shapes of mineralogical endmembers, which display sufficient spectral contrast such that the band math approach is appropriate. This work aims to introduce this methodology for mapping the Bonneville basin with Landsat data, and examines two study areas within the basin over time from 1986 to 2016 to explore changes observed throughout the basin over decadal timescales. Establishing an easily reproducible method for direct mapping of predominant mineralogies in the Bonneville basin will help to facilitate future investigations into the surface sediment distribution of evaporite minerals through time and into the processes and dynamics of evaporite basins globally.

2 | MATERIALS AND METHODS

2.1 | Spectroscopy

Representative surface samples were acquired from associated research on the Bonneville Salt Flats region from 2013 to 2020 and allow for an assessment of the spectral characteristics present in endmember mineralogies of the Bonneville basin. Past research included mineralogical verification of Bonneville basin surface

samples using X-ray diffraction (XRD), elemental geochemistry, and diagnostic textural and petrographic characterization (Bowen *et al*., 2017; Bowen *et al*., 2018). The three mineralogical endmembers considered here (e.g., halite, gypsum, and carbonate) describe the dominant mineralogical content, rather than a pure mineralogical endmember. Although reference spectra for the mineralogies within the basin are found in the US Geological Survey (USGS) Spectral Library, they do not account for moisture content found in field samples or spectral mixing of endmembers (Kokaly *et al*., 2017). Assessment of endmember spectral characteristics is necessary for identifying spectral features of interest to be accentuated by band math operations. These samples were not used to spatially validate or specifically classify the data for this study, but rather to provide additional spectral information to help produce, inform, and interpret the band math indices. Laboratory spectra of field samples were acquired utilizing the Analytical Spectral Devices (ASD) Fieldspec 3 portable spectroradiometer alongside the ASD Contact Probe to avoid illumination and atmospheric variables. A total of 18 samples from various sites throughout the Bonneville Salt Flats region, some with known composition from previous mineralogical analyses, were ground with a ceramic mortar and pestle then placed in plastic trays for viewing, where measures were taken to ensure the plastic trays were not viewed by the spectroradiometer. During the sampling procedure each sample spectra were averaged for 5 s. Every 10 min the spectroradiometer was calibrated using a Spectralon® diffuse reflectance plate. Image endmember spectra are acquired from a Landsat image taken on August 27, 2016 of the Bonneville basin, choosing spectra from areas where the mineralogical endmember is known (Bonneville Salt Flats for halite, Knolls Dunes for gypsum, and the distal rim of the Bonneville Salt Flats for carbonates).

Halite on the Bonneville Salt Flats is predominantly moist; thus, halite samples were analyzed under both dry and wet conditions. If conditions were to become dry such that the salt crust dries out completely, it would be expected to see a flat slope from the near-infrared (NIR) to short-wave infrared (SWIR)-1 band, although dry halite field samples show a gentle negative slope (Figure 3b). The amount of absorption increase from the NIR to SWIR-1 band for halite correlates with the degree of moisture. All samples used for spectroscopy were acquired months-to-years prior to obtaining their spectra and were thus preliminarily dry. Halite samples were wetted to saturation using distilled water subsequent to obtaining dry spectra. Sample spectra are compared to laboratory spectra of the USGS Spectral Library and previous literature which characterize absorption features of halite, gypsum, and carbonates (Hunt, 1977; Clark *et al*., 1990; Crowley, 1991; Clark, 1999; Gendrin, 2005; Kokaly *et al*., 2017; Wang *et al*., 2018).

Absorption bands at ~1430 and ~1930 nm are most prominent for field halite samples as well as subtle absorption bands at ~990, ~1190, and ~1740 nm, which are all seen in gypsum spectra (Hunt, 1977; Clark *et al*., 1990; Crowley, 1991; Kokaly *et al*., 2017). All of these absorption features, except for the feature at ~1740 nm, are due to overtone(s) and combination(s) of the fundamental vibrational frequencies of water, which is present in the crystal structure of gypsum ($CaSO_4{\cdot}2H_2O$). The presence of these features in the dry samples indicate the field halite samples are not significantly pure halite (NaCl), as pure halite has no absorption features in the visible and near-infrared (VNIR) due to a lack of fundamental vibrations (Hunt, 1977; Clark, 1999). Wet halite shows enhanced absorption in the NIR-SWIR due to the strength of the water absorption features located near 1400 and 1900 nm. The enhanced absorption in the NIR-SWIR region matches what is observed for halite in the image spectra, indicating the halite throughout the Bonneville basin is wet. Dry halite does not match the spectral characteristics of halite in the Bonneville basin. Gypsum spectra show absorption bands at ~990, ~1190, ~1440, ~1740, and ~1930 nm which are consistent with previous characterizations of gypsum spectra (Hunt, 1977; Clark *et al*., 1990; Crowley, 1991; Gendrin, 2005; Kokaly *et al*., 2017). The gypsum absorption feature at ~1440 is a triplet, where three absorption features at ~1440, ~1484, and ~1530 nm constitute a large absorption feature. Carbonate spectra show considerable amounts of variability, likely due to the abundance and diversity of phyllosilicates present, but share absorption bands near 1420, 1920, and 2200 nm. The absorption features near 1420 and 1920 nm are likely due to water, while the feature near 2200 nm is likely due to the presence of Al-OH from clays (Hunt, 1977; Clark *et al*., 1990). The diagnostic carbonate absorption feature near 2350 nm, originating from overtones and vibrational combinations, is outside the wavelengths captured by Landsat sensors, thus the indices rely on overtones and general shape of the spectral hull (Hunt, 1977). Some carbonate samples contain noticeable broad and shallow absorption features near 1100 nm, likely due to electronic processes as it is not due to water or carbonate vibrational absorption processes (Hunt, 1977; Clark *et al*., 1990; Wang *et al*., 2018). Laboratory spectra were downsampled with Harris Geospatial's ENVI 5.5.2 software to the specifications of the Landsat Operational Land Imager (OLI) sensor for the purpose of comparing laboratory and image spectra. Comparisons of spectra (Figure 3) illustrate similarities between laboratory and image spectra. However, when comparing gypsum image spectra to laboratory spectra, there is strong agreement with the mixed halite-and-gypsum spectra. This suggests the gypsum endmember is generally a gypsum-halite mixture, which is consistent with previous geochemical analysis of the salt crust (Bowen *et al*., 2018). Furthermore, the negative slope seen from the NIR to SWIR-1 bands for pure and dry halite, along with absorption features present, indicate the halite is mixed with a hydrated mineral. XRD analysis of a dry halite sample that visually appears pure (crystalline and white) shows that there are traces of gypsum present in field samples that initially appear very pure (see Supporting Information, Figure S1). Although XRD recognizes halite to be the dominant mineral in the sample, when the sample is observed through VNIR spectroscopy the spectral features due to gypsum (water absorption) are very strong, exemplifying non-linear mixing. Thus, there is gypsum in the halite and halite in the gypsum present within the Bonneville basin, and the spectral mixing of these endmembers is non-linear resulting in strong water features even for predominantly pure halite.

2.2 | Remote sensing data collection and pre-processing

Optical sensors utilized are the Landsat-8 OLI and Landsat-5 Thematic Mapper (TM) sensors, which share adequately similar sensor spectral

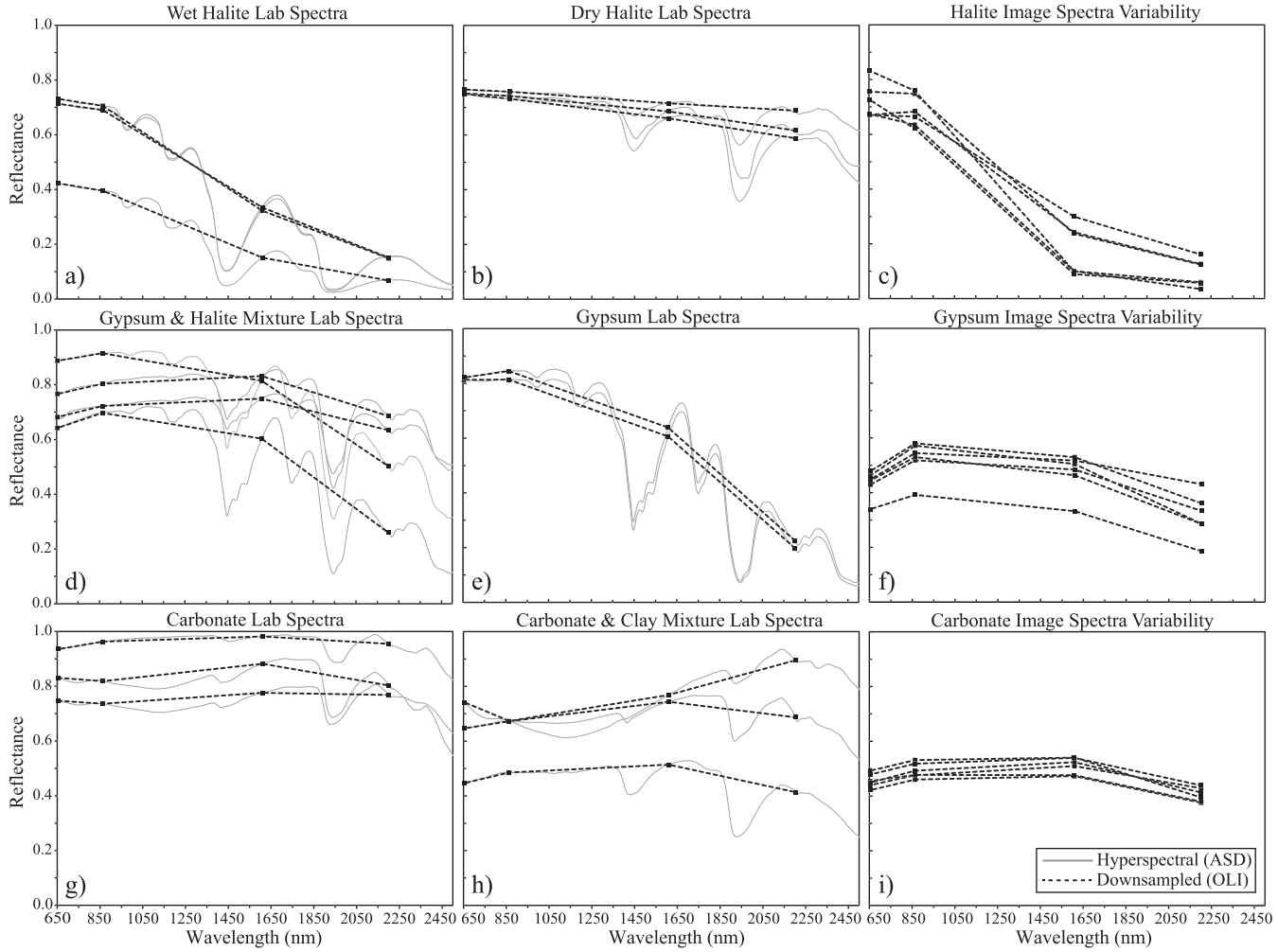

FIGURE 3 Laboratory and image spectra of mineralogies from Bonneville basin, from 650 to 2500 nm, where the laboratory spectra are shown as acquired from the ASD (solid gray line) as well as downsampled to Landsat-8 OLI specifications (black dashed line). Black squares represent Landsat OLI band locations, where the first square at 650 nm is the red band. Plots (a–c) are halite, plots (d–f) are gypsum, and plots (g–i) are carbonates

resolution (VNIR-SWIR), 30 m spatial resolution, and 185 km × 180 km scene sizes. Landsat satellites 6 and 7 were not used as Landsat-6 had a transient life-span and Landsat-7 has corrupted scenes due to a permanent scan line corrector failure which occurred in 2003 (Lee *et al*., 2017). Additionally, the choice to use Landsat TM and OLI instead of ASTER (Advanced Spaceborne Thermal Emission and Reflection Radiometer), or other similar multispectral satellites, is based around Landsat's ability to fully capture the extent of the study area(s) in a single day. ASTER scenes are 60 km × 60 km, which would require three passes (over 1 month of acquiring imagery) of the sensor over the Bonneville basin to create a mosaic of the full basin. One of the main motivations for this study is to present an optical method which can image the entire surface sediment distribution of the Bonneville basin on a single day (one pass over the basin). By utilizing Landsat data, image mosaics (stitching of two or more scenes) are thus composed of images from the same date, as Landsat is able to image the entire Bonneville basin in one pass. Additionally, ASTER was not chosen because the imager was placed into orbit in 1999 and the SWIR sensors became unusable in 2008, which does not allow for current and/or long-term surface sediment distribution investigations (JPLJ, 2008). Level-1 Landsat TM and OLI data (USGS, 2013) were acquired through USGS's Earth Explorer website (www.earthexplorer.com) where cloudless scenes were selected during peak time of desiccation (July/August for Northern Hemisphere) for the best possibility of avoiding standing water and/or high amounts of surface moisture (Bowen *et al*., 2017). Scenes for the Bonneville basin correspond to Landsat path 39 and rows 31 and 32. Chosen scenes were imaged on dates to achieve approximate decadal comparisons from the 1980s to 2010s: August 25, 1986, August 18, 1995, August 29, 2005, August 27, 2016. Years with cloudy images or large amounts of standing water were not used.

Pre-processing of the Landsat imagery follows atmospheric correction, dark object subtraction, mosaicking of images, and isolation of surface deposits. Atmospheric correction was achieved utilizing Fast Line-of-Sight Atmospheric Analysis of Hypercubes (FLAASH), which utilizes MODTRAN® and has been used for multispectral mineralogical studies with satisfactory performance (Anderson *et al*., 2003, 2008; Kayadibi, 2011). Mosaicking of images, and all subsequent image processing, was performed with ENVI 5.5.2. Surface basin deposits were isolated by masking bedrock, vegetation, and standing water. Bedrock surrounding and within the basin was mapped and masked manually, referencing the August 27, 2016

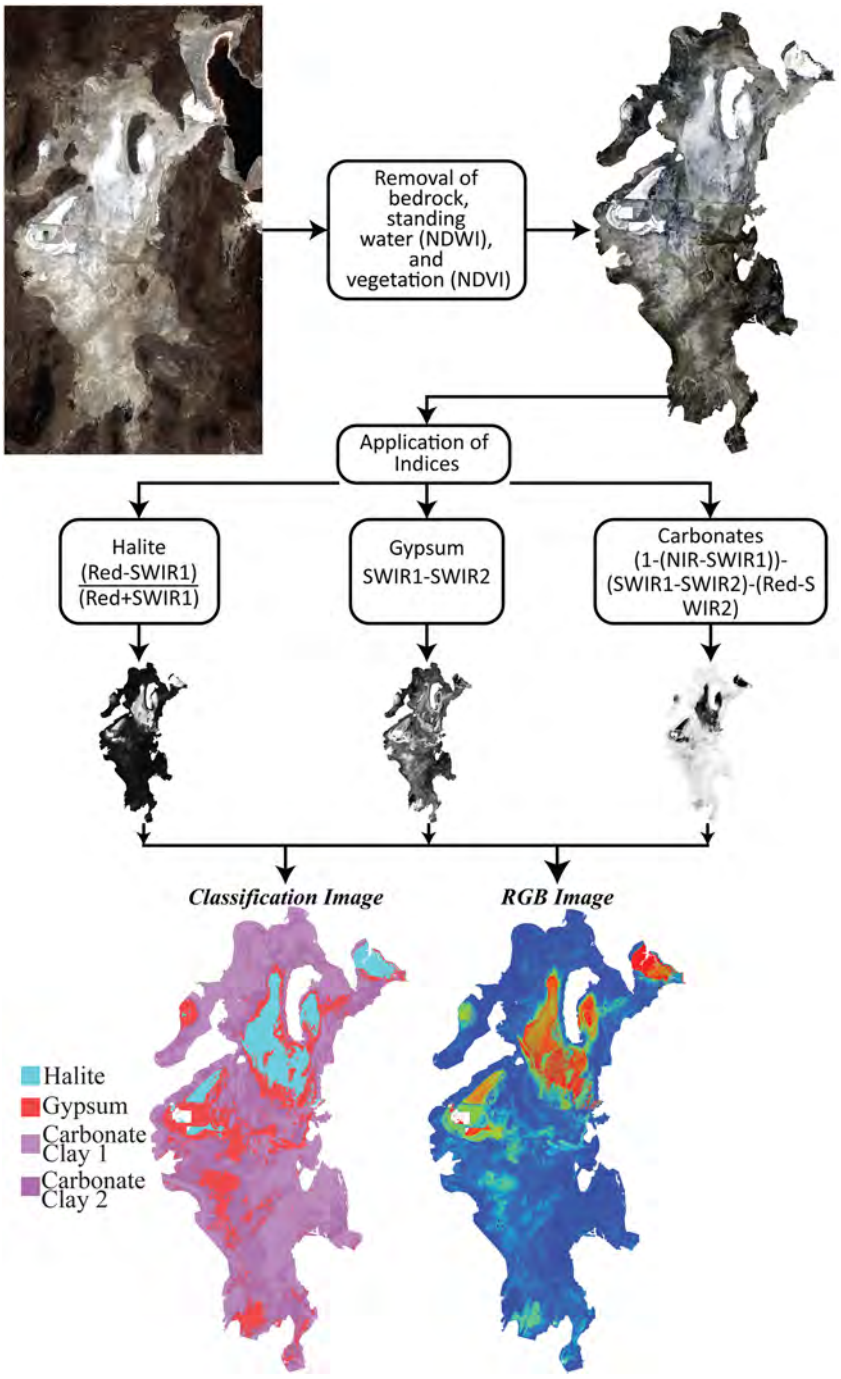

FIGURE 4 Workflow diagram illustrating the processing pathway used for the production of classification and RGB images utilizing the established band math indices

Landsat-8 OLI image as well as a geological map (Hintze *et al*., 2000). The Normalized Difference Vegetation Index (NDVI) and Normalized Difference Water Index (NDWI) were used to isolate and mask vegetation and water (Rouse *et al*., 1973; Bocai, 1996; Ji *et al*., 2009). Thresholds for NDWI were chosen by referencing the Great Salt Lake and other known bodies of water, while NDVI thresholds were chosen as 0.2 to detect shrub as well as healthy vegetation (Gandhi *et al*., 2015). The majority of masked pixels belong to water or bedrock, as very little vegetation was detected.

2.3 | Band math indices

The fundamental objective for manually generating band math indices is to identify unique spectral characteristics to be exploited. Thus, producing the presented band math indices began as a theoretical and inquisitive process, inspecting differences in spectra from spectral databases and devising a way to separate the spectral features. Once an initial set of indices were produced from investigating spectral databases, spectra from the field were utilized for optimization. For the Bonneville basin, three endmember mineralogies, halite, gypsum, and carbonate, are common across the surface and all provide sufficiently differing spectral features to differentiate. Spectral features observed for identification of halite specific to the Bonneville basin is a strong increase in absorption from bands Red to SWIR-1 due to the presence of water and/or gypsum. Gypsum in the Bonneville basin illustrates a slight increase in absorption from bands NIR to SWIR-1, but most notable is a strong increase in absorption from SWIR-1 to SWIR-2 that is rarely observed with the other endmember samples. Carbonate-clays of the Bonneville basin show the least amount of variability from NIR to SWIR-1, usually

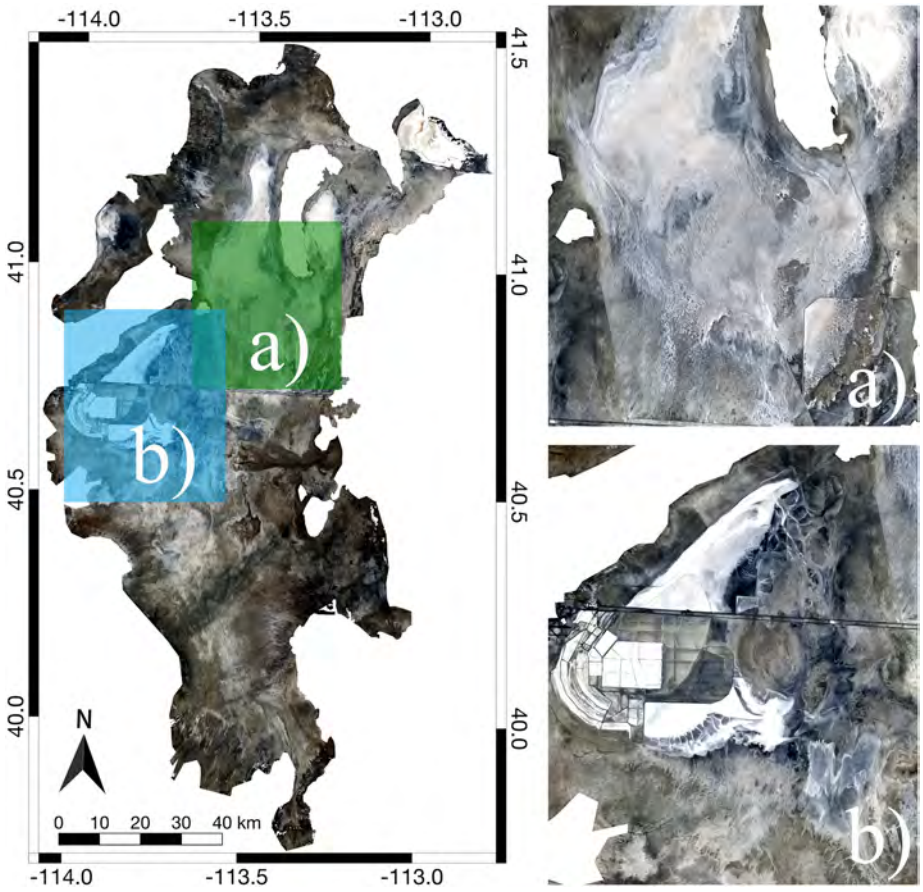

FIGURE 5 Map of isolated (masked bedrock, vegetation, and water) Bonneville basin surface sediment deposits with boundaries defining the study areas (a) the Newfoundland basin, and (b) the Bonneville Salt Flats. Datum is WGS 84 EPSG:32612

having a slight decrease in absorption for SWIR-1, which is utilized in the index. These spectral features, which form the basis by which the indices are able to separate endmember mineralogies, are unique to each endmember but are also reliant on the environmental conditions and mineralogical mixtures of the Bonneville basin. The halite and gypsum indices accentuate these endmembers by directly separating out the spectral features of interest. In contrast, the carbonate index acts by accentuating spectra that show the least amount of variability from NIR to SWIR-1 as well as subduing spectra with features representative of halite or gypsum. Improvement of the indices was an iterative process utilizing theoretical calculations, such that improvements to the indices resulted in further amounts of spectral contrast. The established band math indices for accentuation of mineralogical endmembers of the Bonneville basin are shown in Equations 1–3:

$$\textbf{\textit{Halite}}: \frac{Red - SWIR1}{Red + SWIR1}, \tag{1}$$

$$\textbf{\textit{Gypsum}}: SWIR1 - SWIR2, \tag{2}$$

$$\textbf{\textit{Carbonates}}: (1 - (NIR - SWIR1)) - (SWIR1 - SWIR2) - Red - SWIR2 \tag{3}$$

Implementation of the indices results in grayscale images where the brightest pixels are pixels of interest and represent the mineralogical endmember associated with the index. These output images can be used for classification maps or RGB composite image maps where R = halite, G = gypsum, and B = carbonate (Figure 4). Classification maps are beneficial in that they discretely categorize pixels as a specific class or endmember and can be used to calculate surface area or relative percentages of endmembers. Additionally, classification maps provide more generalized information and are consequently easier to read. RGB composite image maps are useful in that they display more detailed information, which can be used to investigate surface dynamics, and provide insight into areas of mineralogical mixing. RGB maps presented utilize a linear contrast stretch. The generation of classification maps for this study utilized manual thresholding of the indices output images to isolate pixels of interest (pixels with values above the threshold). Alternative thresholding methods exist, including automatic methods, but for the scope of this study those methods are not utilized or reviewed.

For standardization, the thresholds chosen are based on histogram percentiles of each index output image. For halite, the thresholds between the 85th and the 95th histogram percentile most optimally captures extent. Therefore, decades between 1986 and 2016 utilized halite thresholds of the 95th, 85th, 85th, and 90th histogram percentiles, respectively. Thresholds for gypsum are found to be optimal between the 80th and the 90th histogram percentiles, where the thresholds chosen from 1986 to 2016 are the 89th, 92nd, 92nd, and 80th percentiles, respectively. Finally, thresholds for carbonates are split into two, as the output grayscale images display two tiers of bright pixels, suggesting there are two subclasses of carbonates to be distinguished. Carbonate thresholds are thus found to be optimal when chosen at the 20th and 60–85th histogram percentiles. Thresholds chosen from 1986 to 2016 for the carbonates are the 15th and

TABLE 1 Confusion matrix results (in percentages) of the ground truth regions of interest (ROIs) (left column), determined utilizing ASTER imagery from 2005, compared to the 2005 Landsat classification map (top row). Unclassified pixels occur due to pixels which are classified as ground truth ROIs but correspond to masked pixels in the image classification map (i.e., water or vegetation)

Confusion matrix results (percentage)				
Class	**Halite**	**Gypsum**	**Carbonate**	**Total**
Halite	99.65	0	0	58.43
Gypsum	0.35	75.07	0.28	8.64
Carbonates	0	22.24	99.69	32.63
Unclassified	0	2.69	0.02	0.31
Total	100	100	100	100
Overall accuracy = 96.93%			κ = 0.9441	

65th, 25th and 68th, 57th and 86th, and 20th and 60th histogram percentiles, respectively (where the first percentile is the lower bound of the first subclass).

2.4 | Study areas for temporal analysis

Two study areas (Figure 5) are mapped temporally to illustrate the output maps as well to initiate discussion regarding the general dynamics within the basin. Study area (a), the Newfoundland basin, provides the opportunity to investigate the evolution of the anthropogenic halite crust that formed as a result of the Great Salt Lake pumping project as well as adjacent gypsum deposits. Study area (b), the Bonneville Salt Flats, is a zone of large anthropogenic impact due to land use and extraction, and provides an opportunity to investigate shrinking crust extent and gypsum zonation. Although more detailed investigations of salt crust extent during the period of comparisons has been performed (Bowen *et al*., 2017), revisiting the Bonneville Salt Flats with the methods presented here provides a test of the methods used in previous work and places understanding of the processes seen at the salt flats within the broader context of the overall basin.

3 | RESULTS

3.1 | Validation of band math indices

To test the indices ability to map surface mineralogical units, four methods of assessing the indices performance are implemented: (1) assessment of index classification accuracy with a confusion matrix, (2) analysis of resulting values when indices are applied to field sample spectra, (3) assessment of 2016 map performance based on comparisons with field samples, and (4) comparisons to a PCA image of the August 27, 2016 scene (derived from the first three output PCA bands). To assess the accuracy of the index derived classifications it is necessary to utilize some form of ground truth data. Due to the lack of viable hyperspectral datasets ASTER data is utilized for the creation of ground truth regions of interest (ROIs) to be used in a confusion matrix, as ASTER contains four more SWIR bands than Landsat and is thus better suited, but not ideal, for mineralogical identification. Two ASTER scenes (AST 07XT 00308212005183101 20200619144416 4219 and AST 07XT 00308212005183101 20200619144415 4219) captured on August 21, 2005 (8 days apart from the 2005 Landsat image), were utilized

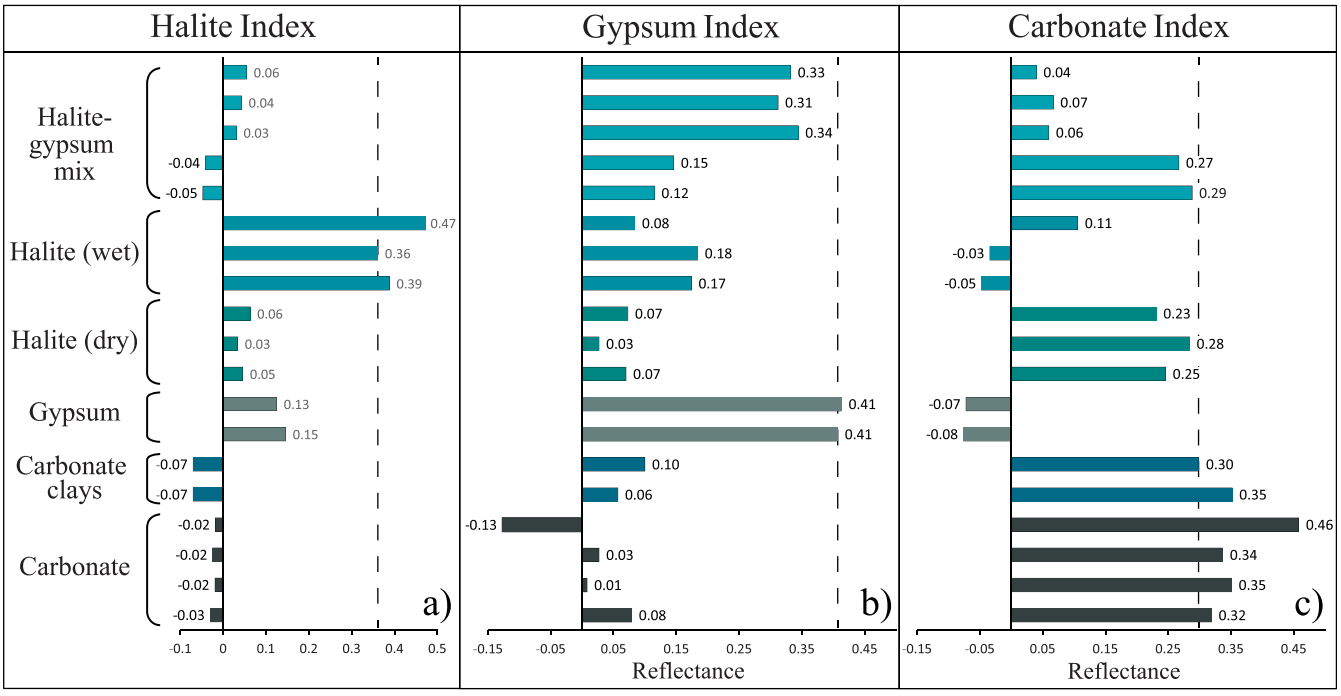

FIGURE 6 Comparison of resulting values after applying each index to sample spectra from Figure 3. Values for halite are dimensionless while gypsum and carbonate values are measured as reflectance. Dashed lines indicate the lowest resulting value from the endmember of focus, illustrating that the endmember of focus will be of larger values (i.e., brighter) than the other endmembers. (a) Resulting values from the halite index, (b) resulting values from the gypsum index, (c) resulting values from the carbonate index

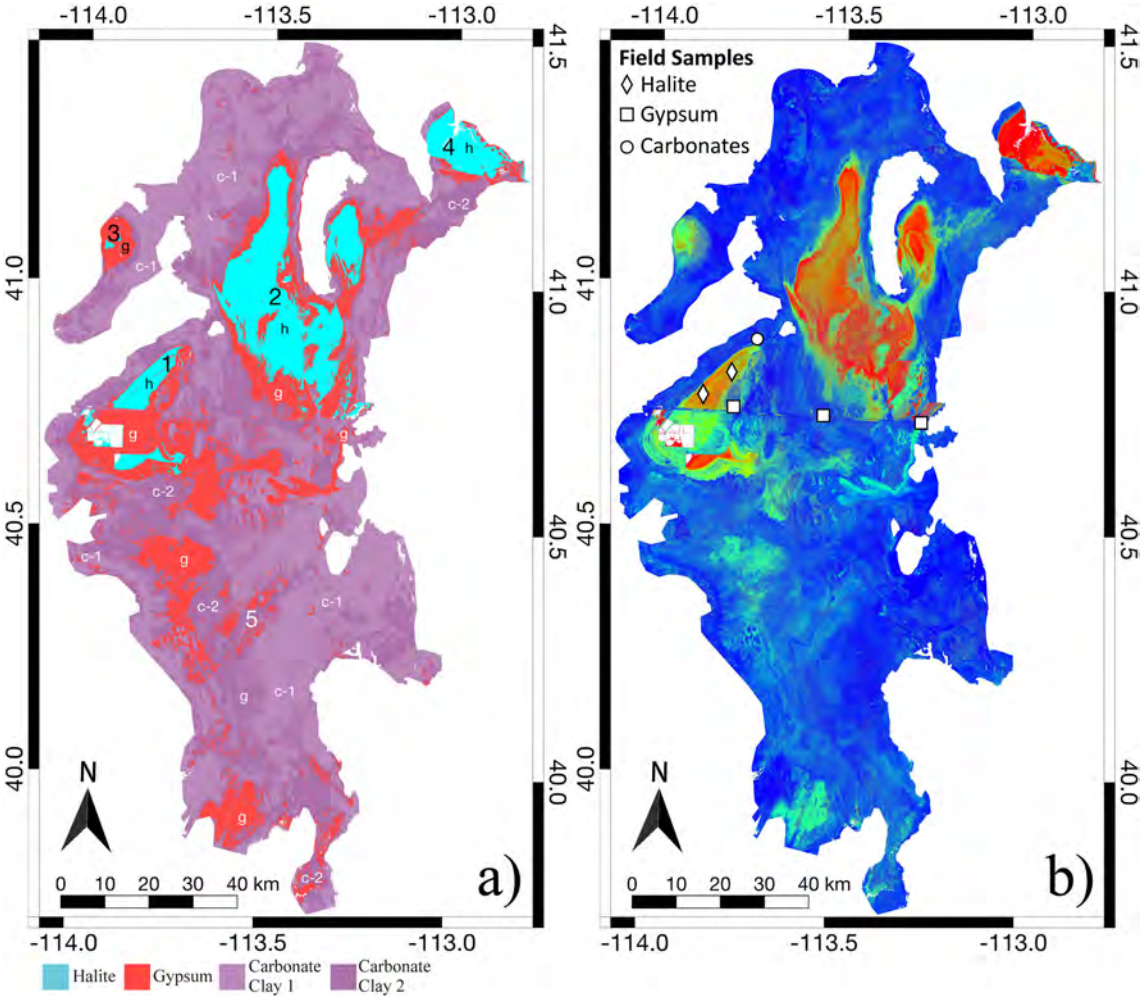

FIGURE 7 Full maps of the Bonneville basin on August 27, 2016 utilizing the presented indices. (a) Classification map with endmember color key underneath. (b) RGB composite image map of linear contrast stretch where R = halite, G = gypsum, and B = carbonates. The RGB map can be interpreted such that bright shades of red indicate halite, shades of green indicate gypsum, and shades of blue indicate carbonates. Field sample locations are overlain, where diamonds are halite, squares are gypsum, and circles are carbonate samples. Due to the close proximity of sampling, one shape can represent up to four samples. Datum is WGS 84 EPSG:32612

(NASA/METI/AIST/Japan Spacesystems and US/Japan ASTER Science Team, 2006). Laboratory spectra (from Figure 3) were down-sampled to ASTER specifications for referencing when determining ground truth ROIs for halite, gypsum, and carbonates. A total of 143,694 pixels (129 km^2) encompass the ground truth ROIs used for calculation of the confusion matrix, which were chosen very conservatively to ensure as accurate of ground truth regions as possible given the limitations. The confusion matrix results (Table 1) indicate an overall accuracy of 96.93% with a kappa coefficient of 0.9441, where 99.65% of halite, 75.07% of gypsum, and 99.69% of carbonate ground truth pixels were correctly classified. These preliminary results suggest the indices work moderately well at classifying each endmember, but shows that the gypsum index may include some carbonates. Although the confusion matrix shows promising results, the ASTER image is temporally separated from the Landsat classification image by 8 days and may inherently be flawed as a ground truth comparison as the surface sediment distribution is likely slightly different. More importantly, utilizing ASTER, or any multispectral sensor, to retrieve mineralogical ground truth regions can be problematic due to the lack of detailed spectral data. Thus, given the limitations of available data, it is required to present less meaningful validation techniques. Although there is no reliable ground truth data to confidently validate the indices at this time, it should be noted that the purpose of these indices is to be used in conjunction to understand general surface dynamics and processes rather than investigate the presence of a specific mineral.

Comparing resulting values from the indices applied to field sample spectra (Figure 6) from Figure 3 provides insight as to how strongly the indices separate the subtle difference in spectral shapes, as the actual resulting contrast of values may be inspected. The results show the halite index very strongly accentuates wet halite, such that gypsum and carbonates values are relatively small or less than zero, while the values for halite are much larger than zero. Dry halite is not accentuated greatly. Values for the halite index are dimensionless, due to the embedded normalization, while the gypsum and carbonate indices result in values measured in reflectance. The resulting values for the gypsum index illustrate accentuation of gypsum, however, the difference of gypsum values between the mixed halite and gypsum values are somewhat small. The small difference in values indicates it is likely that halite with robust spectral gypsum features will be classified as gypsum. The carbonate index values also show that carbonate samples have the highest values, but contrast of

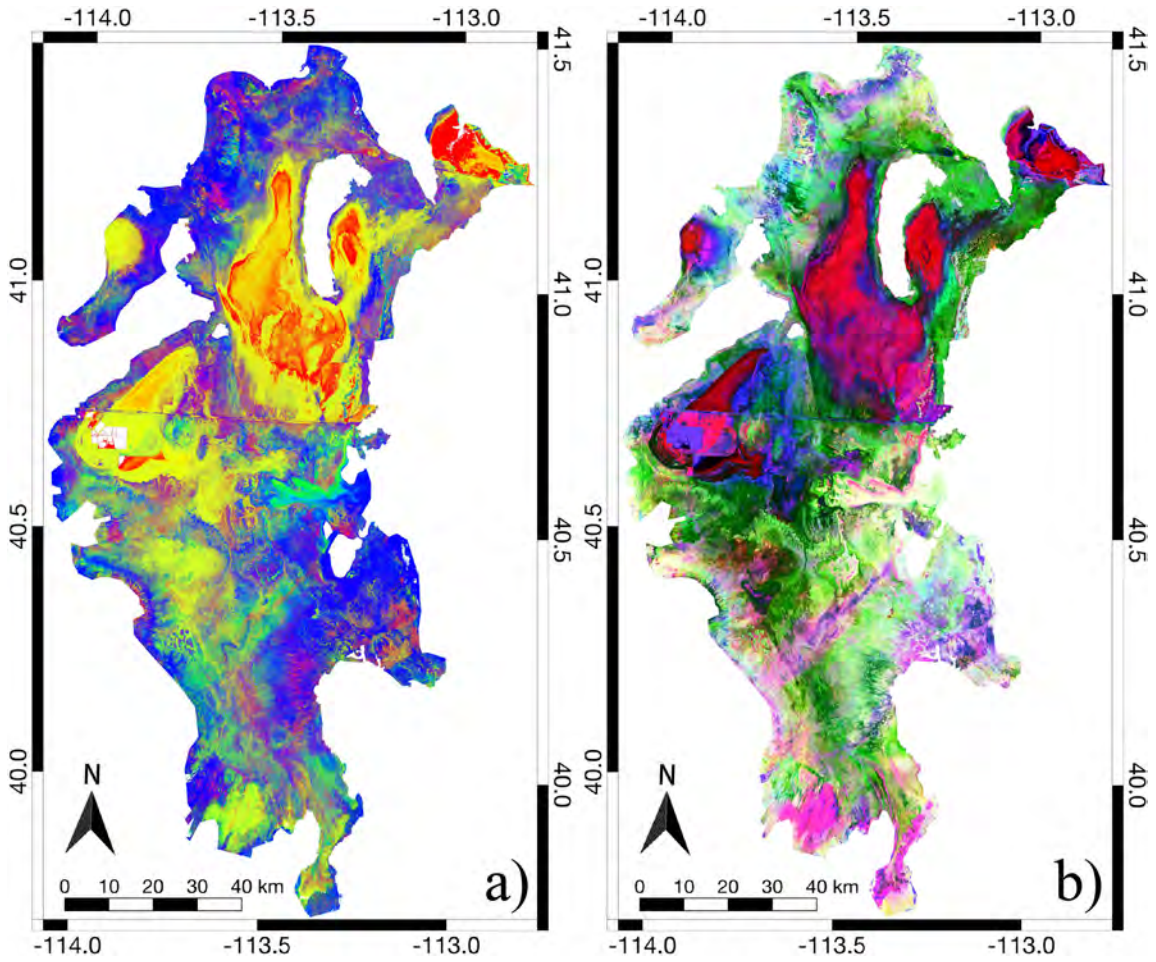

FIGURE 8 (a) Comparisons of the index RGB image (equalized contrast stretch) and (b) RGB principal component analysis image (using the first three bands) derived from the August 27, 2016 Landsat-8 OLI scene. The RGB map (R = halite, G = gypsum, B = carbonates) can be interpreted such that bright shades of red indicate halite, shades of green indicate gypsum, and shades of blue indicate carbonates. Datum is WGS 84 EPSG:32612

values between some mixed halite and gypsum as well as dry halite suggests the possibility of falsely accentuating dry halite or mixed halite and gypsum. These results indicate the indices effectively accentuate the endmember of focus for each index, but there are limitations and possibilities for false-positive identification. Thus, it is encouraged that these indices are not to be used individually but in conjunction, as together they more accurately help understand the general surface sediment distribution. Additionally, the low contrast between select samples for the gypsum and carbonate index suggest that stacking the index images as an RGB image may be more accurate than a classification scheme, as it can be difficult to identify a correct threshold when creating a classification image.

Samples taken from the field are used for assessing the general performance of the final maps. By taking the location and identity of each sample and comparing to locations on the 2016 maps a general ground truth assessment can be presented. All of the 17 samples retrieved were collected from deposits proximal to I-80, on the Bonneville Salt Flats, or directly proximal to the Bonneville Salt Flats. Samples are temporally separated from the 2016 comparison map as they were retrieved at different times. Upon comparison it is observed that all 17 field samples correspond to the endmember identified on the maps (Figure 7b), supporting the indices general applicability.

The output PCA of the August 27, 2016 Landsat-8 OLI scene compared with the index RGB image provides an opportunity to compare the indices performance with an independent method. The comparisons (Figure 8) show predominantly analogous distributions which supports the indices capacity to differentiate surface units. However, some disagreement exists in the southern part of the basin, which is most likely produced due to index confusion from the presence of dry vegetation (desert shrub) that is not prominent in the northern part of the basin and was not detected/masked by the initial NDVI treatment. Overall, the combination of these validation results suggest the indices are able to successfully accentuate differences that are consistent with the mineralogical endmembers present within the Bonneville basin and should be considered suitable for mapping of surface sediment distribution through time.

3.2 | Classification and RGB maps

Prior to investigating temporal comparisons of the chosen study areas, a brief overview of surface sediment distribution for the 2016 classification and RGB maps is discussed. RGB maps can be interpreted such that bright shades of red indicate halite, shades of green indicate gypsum, and shades of blue indicate carbonates. The

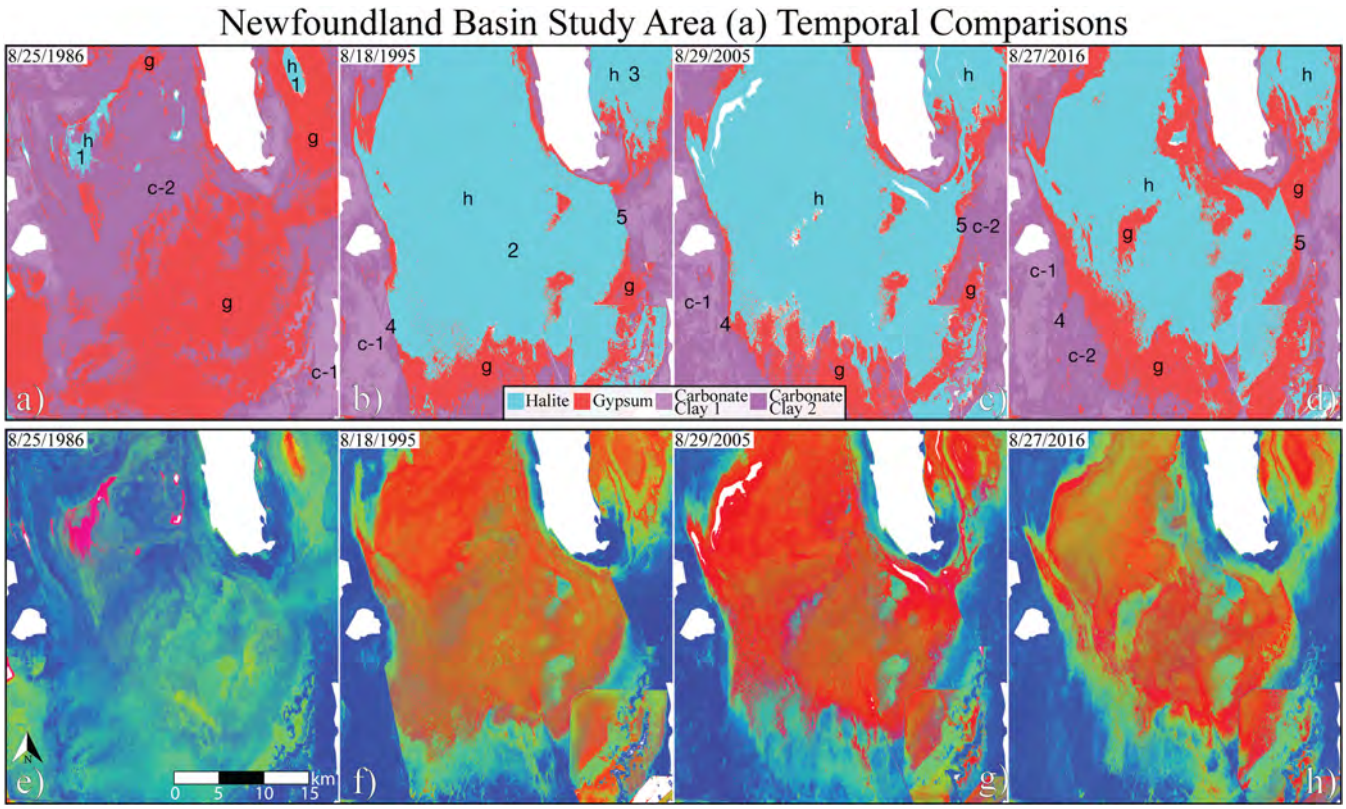

FIGURE 9 Temporal comparisons of study area (a) the Newfoundland basin from 1986 to 2016. Maps (a–d) are classification maps, with the endmember color key below. Maps (e–h) are RGB image composite maps. R = halite, G = gypsum, and B = carbonates. Text symbols are used to denote locations of endmember units for easier image accessibility, where h = halite, g = gypsum, c-1 = carbonate-clay 1, and c-2 = carbonate-clay 2. Text numerals are also present, denoting areas of interest which are discussed in the text

resulting Bonneville basin maps (Figure 7) show that halite and gypsum deposits are generally restricted to the central and northern regions of the basin, where gypsum zones the perimeter of each halite crust present. The large gypsum "sandbox" deposit south of the Bonneville Salt Flats halite crust as well as the Knolls gypsum dunes are apparent and consistent with field observations. Halite crusts are observed at the Bonneville Salt Flats (Figure 7, location 1), Newfoundland basin (Figure 7, location 2), Pilot Valley (Figure 7, location 3), and north-eastern arm of the basin (Figure 7, location 4). Although predominantly restricted to the central and northern region of the basin, isolated gypsum deposits are observed in the southern region of the basin (Figure 7, location 5). Carbonate deposits are scattered throughout, as the evaporites are overlying the carbonates, but dominate the southern section of the basin. Northeast–southwest oriented lineation's are observed traversing the Dugway Proving Grounds region of the basin, and are consistent with wind observations in the area, suggesting wind events greatly affect the southern portion of the Bonneville basin.

3.2.1 | Study area (a) Newfoundland basin

Decadal comparisons of surface sediment distribution at the Newfoundland basin from 1986 to 2016 (Figure 9) provide a unique opportunity to observe the introduction and evolution of a 10-million-ton anthropogenic halite crust. The 1986 surface sediment distribution illustrates the state of Newfoundland basin pre-introduction of the anthropogenic salt crust, which shows predominantly gypsum and carbonates with two small halite crusts bordering the study area (Figure 9, location 1). Following 1989 the Great Salt Lake pumping project ceased and the newly introduced salt crust began to erode.

The study area maps from 1995 to 2016 contain the main portions of the anthropogenic salt crust, and record a dissipation of the southwest corner of the crust through time. In 1995 there are two separated salt crusts (Figure 9, locations 2 and 3) which become connected in 2005 and 2016 by an elongate segment of halite crust, correlating with a northeastward translation of the crust possibly from southwest winds. Dunes composed of gypsum dot the southern crustal body and lower perimeter. Man-made berms cut off the sediments from the southwest and southeast as straight lines (Figure 9, locations 4 and 5), creating sharp contacts between mineralogical endmembers in 1995. The western sharp contact is not seen in 2005 or 2016, as the western halite and gypsum extents retracted away from the berms. Through time the central region of the Newfoundland salt crust exposes the underlying gypsum and carbonates, indicating the crust is likely thinning. Overall, the halite crust is shrinking or being redistributed. Surface area measurements of the entire Newfoundland basin crust from 1986 to 2016, based off halite pixel counts, indicate the anthropogenic crust is shrinking at an average rate of ~14 km^2/yr (Figure 10). Thus, if the crust is indeed thinning and shrinking at a constant rate, it is possible the crust may disappear by the end of the century given the observed rate of crustal area loss. Additionally, surface area measurements from 1986 to 2016 of halite within the entire

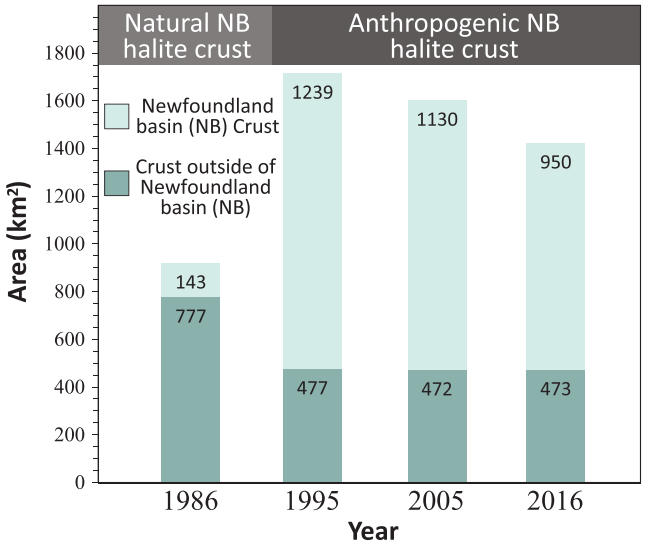

FIGURE 10 Decadal surface area measurements from 1986 to 2016 of halite crusts within the Bonneville basin, graphically illustrating when the Newfoundland basin halite crust grew due to anthropogenic influence after 1986. Values within the bins are the measured surface areas (km^2). A constant decay can be seen from 1995 to 2016 for the anthropogenic crust with an average of ~14 km^2 lost every year, while the natural halite crustal areas outside of the Newfoundland basin appear to have been consistent for the previous three decades

Bonneville basin show the halite crustal area has been consistent outside of the Newfoundland basin for the past three decades. If the Newfoundland basin halite was being redistributed, the overall halite crustal area for the Bonneville basin should be consistent. However, it appears the amount of halite within the Bonneville basin has been decreasing proportionally to the decrease in Newfoundland basin halite. This suggests the Newfoundland basin halite loss is likely due to transport outside of the basin, however, thickness data is required to truly address the halite budget evolution in the Bonneville basin. Gypsum content remains somewhat consistent through time, underlying the crust and sustaining a proximal zonation around the crust. Wind data from the Bonneville Salt Flats, although from 2017 instead of 2016 (weather data is not available for 2016), indicates a significant southwesterly flow which would translate to a similar flow over the Newfoundland basin. Therefore, the smearing pattern of crust migration may be due to wind events. This is particularly relevant as the temporary halite crust may be protecting underlying sediments from aeolian entrainment, and complete erosion or loss of this anthropogenic crust could have significant impacts on air quality in the Salt Lake valley and north-western Utah region.

3.2.2 | Study area (b) Bonneville Salt Flats

Although previous work has studied the Bonneville Salt Flats crust extent from 1986 to 2015 in great detail (Bowen *et al*., 2017), it is worth investigating changes in endmember distribution relative to the shrinking of the halite crust. Initially, it is observed that the crust does not shrink symmetrically, as the crust is dynamically changing year after year (Figure 11). The south-eastern arm of the crust (Figure 11, location 1) appears most affected through time, as the gypsum deposits vary greatly between scenes. Gypsum surrounding the Bonneville Salt Flats were more widespread in 1986, but the relative abundance appears consistent from 1995 to 2016. Although weather data for the Bonneville Salt Flats indicates a predominant southeasterly flow there is a lack of any streak features, indicating the surface sediment distribution of the study area is not significantly changed by wind events. This makes sense, as this salt crust is wet with a higher amount of cohesion in comparison to gypsum dune or carbonate-clay sediments.

4 | DISCUSSION

4.1 | Remote sensing indices and spectroscopy

This study uses multispectral remote sensing to map mineralogy in evaporite basins through time, with a specific focus on the Bonneville basin where monitoring surface sediment distribution is required to quantify land-use implications and assess future landscape changes. Previous studies have utilized supervised/unsupervised classification techniques, band ratioing, decorrelation stretch transformations, and principal component transformations to map evaporite basins (Mohammad *et al*., 2001; Li *et al*., 2014; Flahaut *et al*., 2017; Soltaninejad & Ranjbar, 2018; Gürbüz, 2019; Milewski *et al*., 2020). Here, we present a set of band math indices which allow for direct assessment of a targeted spectral shape for halite, gypsum, and carbonates and establish a reproducible method that can be utilized in the absence of ground truth data. The indices exploit unique spectral features of each endmember mineralogy, effectively accentuating pixels of interest that represent each mineralogical endmember. Due to the limitations of multispectral imagery the indices should be used in conjunction, as there is risk of false identification when interpreting individual index outputs (Table 1 and Figure 6). When combined, the indices provide a strong sense of mineralogical surface sediment distribution and allow for easy-to-interpret products for the monitoring of evaporite basins. Exploiting halite's strong absorption from the Red to SWIR-1 bands, gypsum's strong increase in absorption from the SWIR-1 to SWIR-2 bands, and carbonate's slight drop in absorption from the NIR to SWIR-1 bands form the spectral foundation of the indices. Output images from the indices are grayscale, where the brightest pixels are the pixels of interest (Figure S1). The output images can be utilized for classification maps, where the brightest pixels are isolated through thresholding, or RGB composite image maps where R = halite index output, G = gypsum index output, B = carbonate index output.

Laboratory and image spectral comparisons were used to investigate endmember mineralogies and found that wet halite represents the spectral shape of halite found at the Bonneville basin. Additionally, the spectral comparisons suggest the gypsum present in the Bonneville basin has been reworked and slightly mixed with halite. Validation of indices is assessed through a confusion matrix utilizing ground truth ROIs, application of index calculations using field sample spectra, field sample comparisons with resulting maps, and image comparisons to a PCA image. The confusion matrix results indicate an overall accuracy of 96.93% with a kappa coefficient of 0.9441. Index calculations applied to field sample spectra also

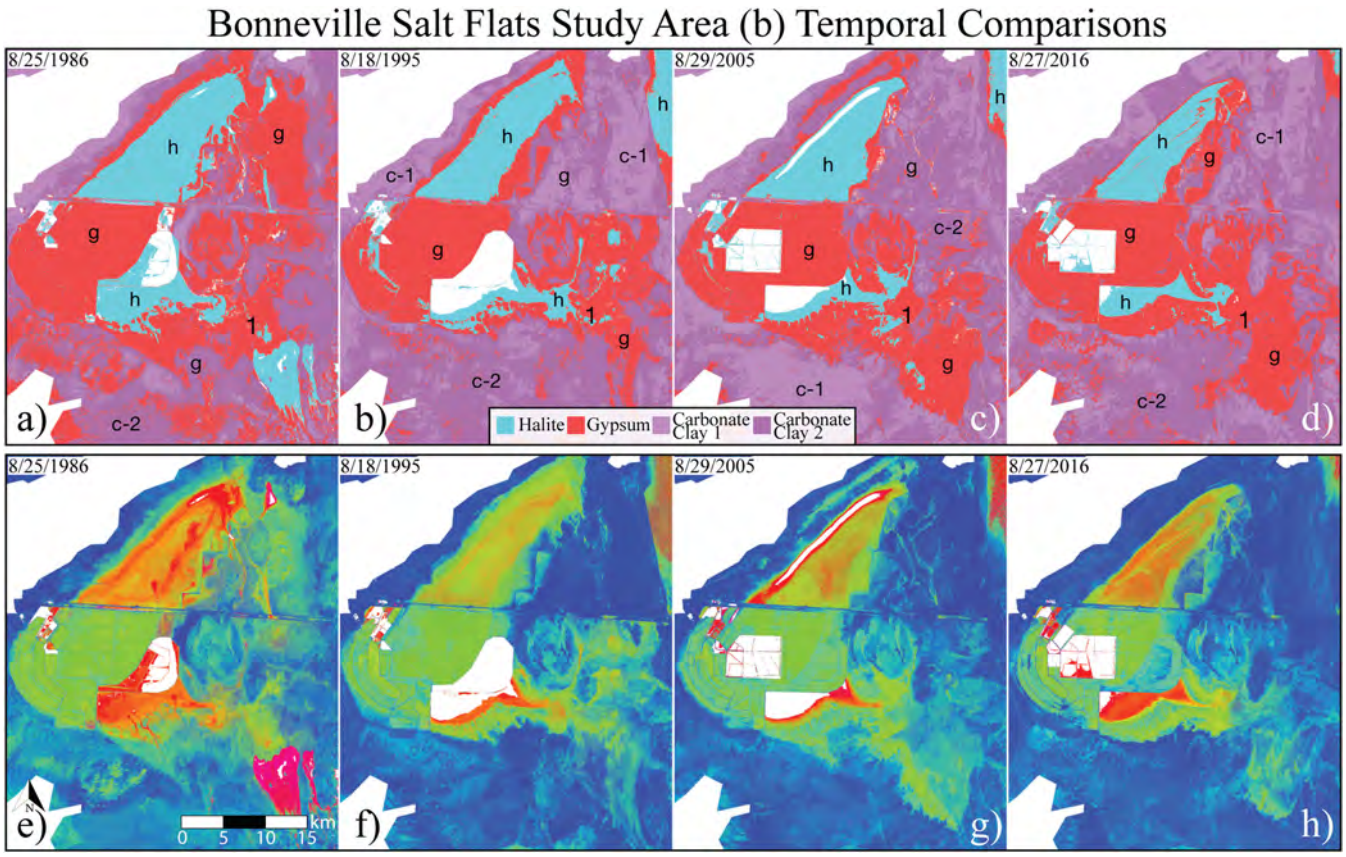

FIGURE 11 Temporal comparisons of study area (b) the Bonneville Salt Flats from 1986 to 2016. Maps (a–d) are classification maps, with the endmember color key below. Maps (e–h) are RGB image maps. R = halite, G = gypsum, and B = carbonates. Text symbols are used to denote locations of endmember units for easier image accessibility, where h = halite, g = gypsum, c-1 = carbonate-clay 1, and c-2 = carbonate-clay 2.. Text numerals are also present, denoting areas of interest which are discussed in the body text

support the general performance of the indices but suggest care should be taken when thresholding for classifications. Comparisons with a PCA image indicate the indices result in surface sediment distributions which agree well with independent methods for differentiating mineralogies. These validation methods suggest the presented set of indices effectively map the general surface sediment distribution of materials in Bonneville basin, although it is probable some materials may be falsely classified. Overall, these indices show value for the use of monitoring surface sediment distribution to better understand evaporite basin dynamics in areas of large anthropogenic influence.

4.2 | Index applicability and case studies

Early studies on evaporite basins concluded there are two types of evaporite basins: wet evaporite basins with shallow hydrological systems and dry evaporite basins with deep hydrological systems (Foshag, 1926; Tyler *et al*., 2006). It has been recognized that groundwater–surface interactions drive geomorphology of evaporite basins and affects mineralogical endmembers at the surface. The Bonneville basin has many shallow-brine aquifers that create a nearly constant moist surface, especially at salt crusts, which inherently classifies the basin as a wet evaporite basin (Lines, 1979; Mason & Kipp, 1998). It is possible the indices established here can crossover to other evaporite basins, but is important to recognize whether the basin is wet or dry as that will determine the spectral characteristics of the endmembers. The presented indices will only be effective in wet evaporite basins where the main mineralogies are halite, gypsum, and carbonates. A few similar evaporite basins are the Salar de Uyuni, Bolivia, and the Lake Eyre, Australia, which are ephemeral basins and illustrate wet halite spectra (Mawson, 1950; Dulhunty, 1974; Orris, 1995; Li *et al*., 2014). For demonstrative purposes, these basins were mapped utilizing the set of indices presented and illustrate sensible endmember distributions (Figure 12). These preliminary results are not supported by any ground observations but could readily be tested given more remote sensing data and/or field data. Furthermore, if hyperspectral imagery is available for a given evaporite basin one can directly assess if the presented indices work for the basin of interest.

Interpretations regarding surface changes within the study areas of the Bonneville basin suggest that further monitoring is needed to better describe spatiotemporal changes of the Newfoundland basin anthropogenic halite crust, the anthropogenic and wind influenced dust sources, and the widely utilized Bonneville Salt Flats. Deeper understandings into the cause and dynamics of surface change at the Bonneville Salt Flats is essential as it is important to balance historical, ecological, and climatic significance with economic and social interests. Implications of studying these areas can help better prepare for local changes in climate, air quality, and hydrological outlooks.

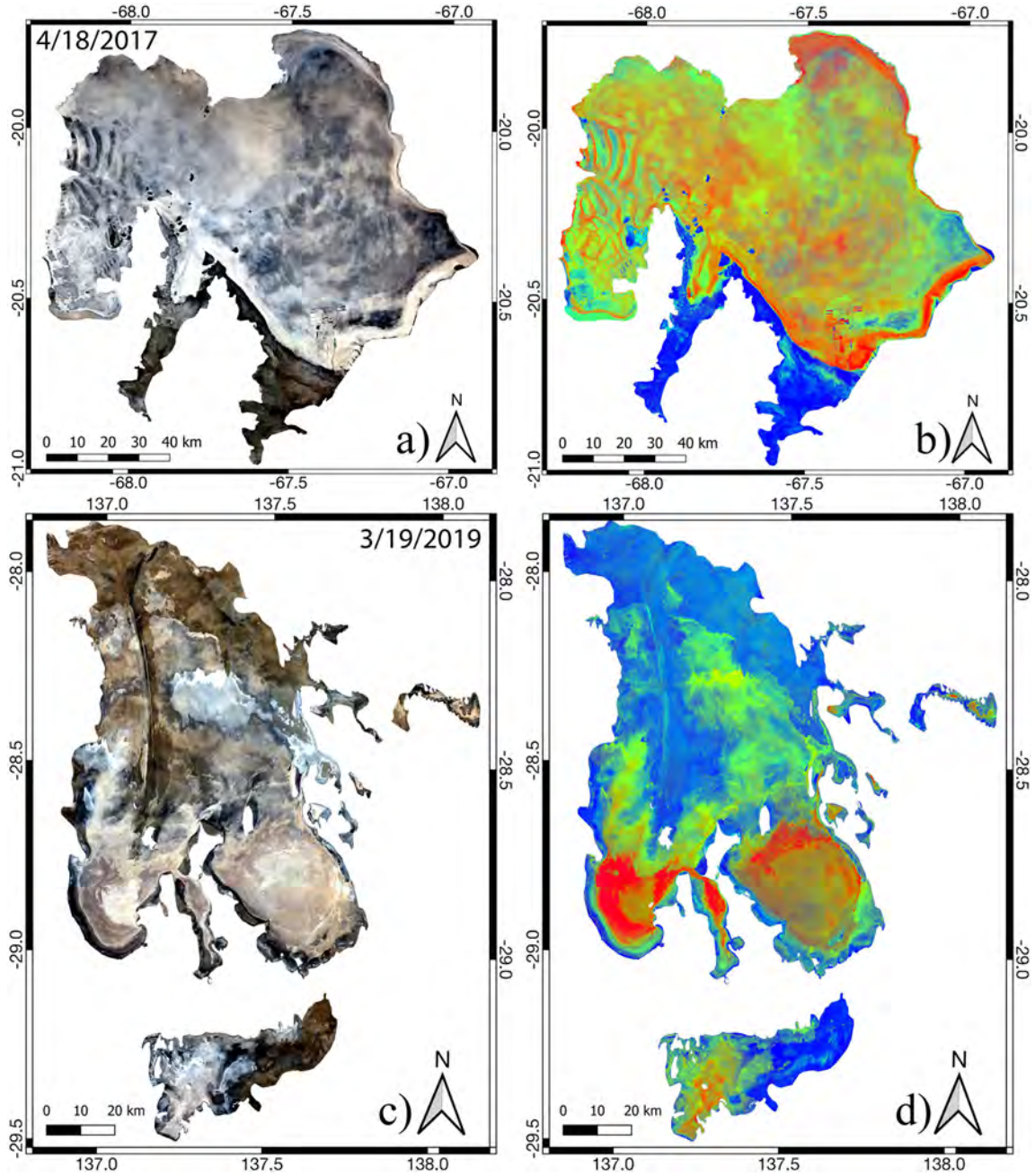

FIGURE 12 Surface sediment distribution maps for the Salar de Uyuni and Lake Eyre evaporite basins. (a) Contextual map of Salar de Uyuni, Bolivia; (b) RGB composite from indices for Salar de Uyuni; (c) contextual map of the Lake Eyre, Australia; (d) RGB composite from indices for Lake Eyre. Datum is WGS 84 EPSG:32612

5 | CONCLUSIONS

This study develops and tests a set of empirical indices to identify halite, gypsum, and carbonates within a wet evaporite basin environment, the Bonneville basin. Examination of the spectral features of evaporites within the Bonneville basin, from laboratory spectra and Landsat image spectra, provided observations of differing spectral characteristics which form the basis of the indices. It is found that the halite present in the Bonneville basin is best represented by wet halite, while the gypsum and carbonate deposits show a lack of water absorption. Additionally, gypsum spectra from Landsat imagery indicate mixing with halite, as seen in comparisons to laboratory spectra of pure gypsum and mixed halite and gypsum spectra. The set of three indices have been preliminarily validated for the accentuation of the predominant mineralogies in the Bonneville basin and allow for the production of classification and RGB composite image maps. The established indices were applied spatiotemporally to observe landscape changes of two study areas within the Bonneville basin. Landsat images used are separated by decades from 1986 to 2016 and have been subset to surface deposits. The study areas of the Bonneville Salt Flats and the Newfoundland basin are both sites of anthropogenic influence from land use and introduction of sediments. Landscape changes are correlated with other phenomenon such as weather and human activities. Although dense time series analysis is needed for quantification of surface processes, it is observed that great amounts of change occur between the maps and much of the change can be directly associated to wind and anthropogenic influence. Correlating events to surface changes can help reveal which

landscape processes respond to change and the magnitude of such responses. Thus, use of the indices may ultimately affect how we understand dust flux, dust sourcing, modifications to the hydrological cycle, impacts of commercial brine extraction, change in surface deposit albedo, introducing sediments, and impact of land use.

ACKNOWLEDGEMENTS

The authors would like to thank Jeremiah Bernau for consultation, reviews, as well as help in acquiring field samples for spectral analysis. Additional appreciation is given to Evan Kipnis and Jory Lerback for extremely valuable input. This research was funded by the National Science Foundation grant number 1617473.

CONFLICT OF INTEREST

The authors declare no conflicts of interest.

6 | DATA AVAILABILITY STATEMENT

The data that support the findings of this study are openly available in the "USGS EROS Archive – Landsat Archives – Landsat 8 OLI (Operational Land Imager) and TIRS (Thermal Infrared Sensor) Level-1 Data Products" repository at https://doi.org/10.5066/F71835S6 as well as in the "ASTER L2 Surface Reflectance VNIR and Crosstalk Corrected SWIR" repository at https://doi.org/10.5067/ASTER/AST_07XT.003.

ORCID

Mark H. Radwin https://orcid.org/0000-0002-7236-1425
Brenda B. Bowen https://orcid.org/0000-0003-3527-3722

REFERENCES

Anderson GP Felde GW, Hoke ML, Ratkowski AJ, Cooley T, Chetwynd, JH Jr., Gardner JA, Adler-Golden S, Matthew MW, Berk A, Bernstein L, Acharya PK 2003. MODTRAN-4 based atmospheric correction algorithm: FLAASH (fast-line-of-sight atmospheric analysis of spectral hypercubes). 65–71 pp.

Anderson GP et al. 2008. FLAASH and MODTRAN4: state-of-the-art atmospheric correction for hyperspectral data. 177–181, 4. https://doi.org/10.1109/aero.1999.792088

Benson, L.V., Lund, S.P., Smoot, J.P., Rhode, D.E., Spencer, R.J., Verosub, K.L., *et al*. (2011) The rise and fall of Lake Bonneville between 45 and 10.5 ka. *Quaternary International*, 235(1-2), 57–69. https://doi.org/10.1016/j.quaint.2010.12.014.

Bo-cai, G. (1996) NDWI—A normalized difference water index for remote sensing of vegetation liquid water from space. *Remote Sensing of Environment*, 58(3), 257–266. https://doi.org/10.1016/s0034-4257(96)00067-3.

Bowen, B.B., Bernau, J., Kipnis, E.L., Lerback, J., Wetterlin, L. & Kleba, B. (2018) The making of a perfect racetrack at the Bonneville Salt Flats. *The Sedimentary Record*, 16(2), 4–11. https://doi.org/10.2110/sedred.2018.2.4.

Bowen, B.B., Kipnis, E.L. & Raming, L.W. (2017) Temporal dynamics of flooding, evaporation, and desiccation cycles and observations of salt crust area change at the Bonneville Salt Flats, Utah. *Geomorphology*, 299, 1–11. https://doi.org/10.1016/j.geomorph.2017.09.036.

Bureau of Land Management. (1986) *West Desert Pumping Project: Final Environmental Impact Statement*. Grand Junction, CO.: Bureau of Land Management.

Clark, R.N. (1999) *Spectroscopy of Rocks and Minerals and Principles of Spectroscopy*. Manual of Remote Sensing.

Clark RN, King TVV, Klejwa M, Swayze GA, Vergo N. 1990. High spectral resolution reflectance spectroscopy of minerals.: 29.

Clark RN, Swayze G, Wise R, Livo KE, Hoefen T, Kokaly R, Sutley SJ. 2007. USGS digital spectral library splib06a. US Geological Survey [online] Available from: http://speclab.cr.usgs.gov/spectral.lib06

Craft, K.M. & Horel, J.D. (2019) Variations in surface albedo arising from flooding and desiccation cycles on the Bonneville Salt Flats, Utah. *Journal of Applied Meteorology and Climatology*, 58(4), 773–785. https://doi.org/10.1175/JAMC-D-18-0219.1.

Crittenden, M.D. (1963) New data on the isostatic deformation of Lake Bonneville. *Geological Survey Professional Paper*, 454-E, 31–31.

Crowley, J.K. (1991) Visible and near-infrared (0.4–2.5 μm) reflectance spectra of playa evaporite minerals. *Journal of Geophysical Research*, 96(B10), 16231–16231. https://doi.org/10.1029/91jb01714.

Dean, L.E. (1978) Aeolian sand dunes of the Great Salt Lake basin. *Utah Geology*, 5.

Dulhunty JA. 1974. Salt crust distribution and lake bed conditions in southern areas of Lake Eyre North. 98th ed. Royal Society of South Australia, Adelaide, Australia: [online] Available from: https://www.biodiversitylibrary.org/item/127779

Eardley, A.J. (1962) *Gypsum Dunes and Evaporite History of The Great Salt Lake Desert*. Salt Lake City, UT.: Utah Geological Survey.

Flahaut, J., Martinot, M., Bishop, J.L., Davies, G.R. & Potts, N.J. (2017) Remote sensing and in situ mineralogic survey of the Chilean salars: An analog to Mars evaporate deposits? *Icarus*, 282, 152–173. https://doi.org/10.1016/j.icarus.2016.09.041.

Foshag, W.F. (1926) Saline lakes of the Mohave Desert region. *Economic Geology*, 21(1), 56–64. https://doi.org/10.2113/gsecongeo.21.1.56.

Gandhi, G.M., Parthiban, S., Thummalu, N. & Christy, A. (2015) Ndvi: Vegetation change detection using remote sensing and GIS – a case study of Vellore district. *Procedia Computer Science*, 57, 1199–1210. https://doi.org/10.1016/j.procs.2015.07.415.

Gendrin, A. (2005) Sulfates in Martian layered terrains: The OMEGA/Mars express view. *Science*, 307(5715), 1587–1591. https://doi.org/10.1126/science.1109087.

Gilbert GK. 1890. Lake Bonneville. US Geological Survey, Reston, VA.

Gill, T.E. (1996) Eolian sediments generated by anthropogenic disturbance of playas: Human impacts on the geomorphic system and geomorphic impacts on the human system. *Geomorphology*, 17(1-3), 207–228. https://doi.org/10.1016/0169-555X(95)00104-D.

Goodman, M.M., Carling, G.T., Fernandez, D.P., Rey, K.A., Hale, C.A., Bickmore, B.R., *et al*. (2019) Trace element chemistry of atmospheric deposition along the Wasatch Front (Utah, USA) reflects regional playa dust and local urban aerosols. *Chemical Geology*, 530, 119317. https://doi.org/10.1016/j.chemgeo.2019.119317.

Gürbüz, E. (2019) Multispectral mapping of evaporite minerals using ASTER data: A methodological comparison from central Turkey. *Remote Sensing Applications: Society and Environment*, 15, 100240–100240. https://doi.org/10.1016/j.rsase.2019.100240.

Hahnenberger, M. & Nicoll, K. (2014) Geomorphic and land cover identification of dust sources in the eastern Great Basin of Utah, U.S.A. *Geomorphology*, 204, 657–672. https://doi.org/10.1016/j.geomorph.2013.09.013.

Hintze LF, Willis GC, Laes DYM, Sprinkel DA, Brown KD. 2000. Digital Geologic Map of Utah, https://doi.org/10.34191/M-179DM

Hunt, G. (1977) Spectral signatures of particulate minerals in the visible and near infrared. *Geophysics*, 42(3), 501–513. https://doi.org/10.1190/1.1440721.

Ji, L., Zhang, L. & Wylie, B. (2009) Analysis of dynamic thresholds for the Normalized Difference Water Index. *Photogrammetric Engineering and Remote Sensing*, 75(11), 1307–1317. https://doi.org/10.14358/PERS.75.11.1307.

Jones, B.F., White, W.W., III, Conko, K.M., Webster, D.M. & Hohler, J.F. (2009) *Mineralogy and Fluid Chemistry of Surficial Sediment in the Newfoundland Basin, Tooele and Box Elder Counties*. Salt Lake City, UT.: Utah Geological Survey.

JPLJ. 2008. ASTER User Advisory. Advanced Spaceborne Thermal Emission and Reflection Radiometer

Kayadibi O. 2011. Evaluation of imaging spectroscopy and atmospheric correction of multispectral images (Aster and Landsat 7 ETM+). RAST 2011. Proceedings of 5th International Conference on Recent

Advances in Space Technologies: 154–159. DOI: https://doi.org/10.1109/RAST.2011.5966811

Kohler, J. (2002) Effects of the West Desert Pumping Project on the near-surface brines in a portion of the Great Salt Lake desert, Tooele and Box Elder Counties, Utah. In: *Great Salt Lake: An Overview of Change*, pp. 487–498.

Kokaly R et al. 2017. USGS Spectral Library Version 7. US Geological Survey, Reston, VA.

Lee, S., Cho, M. & Lee, C. (2017) An Effective Gap Filtering Method for Landsat ETM+ SLC-Off Data. *Terrestrial, Atmospheric and Oceanic Sciences*, 27(6), 921–932. https://doi.org/10.3319/tao.2016.07.18.02.

Li, J., Menenti, M., Mousivand, A. & Luthi, S.M. (2014) Non-vegetated playa morphodynamics using multi-temporal landsat imagery in a semi-arid endorheic basin: Salar de Uyuni, Bolivia. *Remote Sensing*, 6 (10), 10131–10151. https://doi.org/10.3390/rs61010131.

Lines GC. 1979. Hydrology and Surface Morphology of the Bonneville Salt Flats and Pilot Valley Playa, Utah. US Geological Survey Water-Supply Paper **2057**. US Geological Survey, Reston, VA.DOI: https://doi.org/10.3133/wsp2057

Lowenstein, T.K. & Hardie, L.A. (1985) Criteria for the recognition of salt-pan evaporites. *Sedimentology*, 32(5), 627–644. https://doi.org/10.1111/j.1365-3091.1985.tb00478.x.

Lynch, K.L., Horgan, B.H., Munakata-Marr, J., Hanley, J., Schneider, R.J., Rey, K.A., *et al*. (2015) Near-infrared spectroscopy of lacustrine sediments in the Great Salt Lake Desert: An analog study for Martian paleolake basins: Mars Analog Paleolake Spectroscopy. *Journal of Geophysical Research, Planets*, 120(3), 599–623. https://doi.org/10.1002/2014JE004707.

Mason, J.L. & Kipp, K.L. (1998) *Hydrology of the Bonneville Salt Flats, Northwestern Utah, and Simulation of Ground-Water Flow and Solute Transport in the Shallow-Brine Aquifer*. Reston, VA.: US Geological Survey.

Mawson, D. (1950) Occurrence of water in Lake Eyre, South Australia. *Nature*, 166(4225), 667–668. https://doi.org/10.1038/166667a0.

McLaurin, B.T., Goossens, D. & Buck, B.J. (2011) Combining surface mapping and process data to assess, predict, and manage dust emissions from natural and disturbed land surfaces. *Geosphere*, 7(1), 260–275. https://doi.org/10.1130/GES00593.1.

Milewski, R., Chabrillat, S. & Behling, R. (2017) Analyses of Recent Sediment Surface Dynamic of a Namibian Kalahari Salt Pan Based on Multitemporal Landsat and Hyperspectral Hyperion Data. *Remote Sensing*, 9(2), 9. https://doi.org/10.3390/rs9020170.

Milewski, R., Chabrillat, S. & Bookhagen, B. (2020) Analyses of Namibian seasonal salt pan crust dynamics and climatic drivers using Landsat 8 time-series and ground data. *Remote Sensing*, 12(3), https://doi.org/10.3390/rs12030474.

Moersch JE, Farmer J, Baldridge A. 2001. Remote Sensing of Evaporite Minerals in Badwater Basin, Death Valley, at Varying Spatial Scales and in Different Spectral Regions. Workshop on the Martian Highlands and Mojave Desert Analogs

Mohammad MR, El-Sobky H, Sedeik K, El Raey M. 2001. Application of Band Ratios Identified by HHRR for Recognition of Surface Units Using TM Data in SIWA Depression, Western Desert, Egypt. Conference paper presented at the 22nd Asian Conference of Remote Sensing: 5–9.

NASA/METI/AIST/Japan Spacesystems and US/Japan ASTER Science Team. 2006. ASTER On-Demand L2 Surface Reflectance VNIR and SWIR Crosstalk-Corrected [online] Available from: https://doi.org/10.5067/ASTER/AST_07XT.003

Orris GJ. 1995. Bibliography and summary of data available for the Salar de Uyuni, Bolivia

Oviatt, C.G. (1997) Lake Bonneville fluctuations and global climate change. *Geology*, 25(2), 155–158. https://doi.org/10.1130/0091-7613(1997)025%3C0155:LBFAGC%3E2.3.CO;2.

Pelletier, J.D. & Cook, J.P. (2005) Deposition of playa windblown dust over geologic time scales. *Geology*, 33(11), 909. https://doi.org/10.1130/G22013.1.

Quick, D.J. & Chadwick, O.A. (2011) Accumulation of salt-rich dust from Owens Lake playa in nearby alluvial soils. *Aeolian Research*, 3(1), 23–29. https://doi.org/10.1016/j.aeolia.2011.03.004.

Rouse, J.W., Hass, R.H., Schell, J.A. & Deering, D.W. (1973) Monitoring vegetation systems in the great plains with ERTS. *Third Earth Resources Technology Satellite (ERTS) Symposium*, 1, 309–317.

Skiles, S.M.K., Mallia, D.V., Hallar, A.G., Lin, J.C., Lambert, A., Petersen, R. & Clark, S. (2018) Implications of a Shrinking Great Salt Lake for dust on snow deposition in the Wasatch Mountains, UT, as informed by a source to sink case study from the 13–14 April 2017 Dust Event. *Environmental Research Letters*, (12), 13. https://doi.org/10.1088/1748-9326/aaefd8.

Soltaninejad, A. & Ranjbar, H. (2018) Evaporite mineral mapping and determining their source rocks using remote sensing data in Sirjan playa, Kerman, Iran. *Carbonates and Evaporites*, 32, 255–274.

Tyler, S.W., Muñoz, J.F. & Wood, W.W. (2006) The response of playa and sabkha hydraulics and mineralogy to climate forcing. *Ground Water*, 44(3), 329–338. https://doi.org/10.1111/j.1745-6584.2005.00096.x.

USGS. 2013. USGS EROS Archive - Landsat Archives - Landsat 8 OLI (Operational Land Imager) and TIRS (Thermal Infrared Sensor) Level-1 Data Products [online] Available from: https://doi.org/10.5066/F71835S6

Wang, F., Bowen, B.B., Seo, J.-H. & Michalski, G. (2018) Laboratory and field characterization of visible to near-infrared spectral reflectance of nitrate minerals from the Atacama desert, Chile, and implications for Mars. *American Mineralogist*, 103(2), 197–206. https://doi.org/10.2138/am-2018-6141.

SUPPORTING INFORMATION

Additional supporting information may be found online in the Supporting Information section at the end of this article.

How to cite this article: Radwin MH, Bowen BB. Mapping mineralogy in evaporite basins through time using multispectral Landsat data: Examples from the Bonneville basin, Utah, USA. *Earth Surf Process Landforms*. 2021;1–17. https://doi.org/10.1002/esp.5089